

This is the peer reviewed version of the following article:

Bandgap Engineering of Graphene Nanoribbons by Control over Structural Distortion / Hu, Yunbin; Xie, Peng; De Corato, Marzio; Ruini, Alice; Zhao, Shen; Meggendorfer, Felix; Straasø, Lasse Arnt; Rondin, Loic; Simon, Patrick; Li, Juan; Finley, Jonathan J.; Hansen, Michael Ryan; Lauret, Jean-Sébastien; Molinari, Elisa; Feng, Xinliang; Barth, Johannes V.; Palma, Carlos-Andres; Prezzi, Deborah; Müllen, Klaus; Narita, Akimitsu. - In: JOURNAL OF THE AMERICAN CHEMICAL SOCIETY. - ISSN 0002-7863. - 140:25(2018), pp. 7803-7809. [10.1021/jacs.8b02209]

Terms of use:

The terms and conditions for the reuse of this version of the manuscript are specified in the publishing policy. For all terms of use and more information see the publisher's website.

18/12/2025 19:39

Bandgap Engineering of Graphene Nanoribbons by Control over Structural Distortion

Yunbin Hu, Peng Xie, Marzio De Corato, Alice Ruini, Shen Zhao, Felix Meggendorfer, Lasse Arnt Straasø, Loic Rondin, Patrick Simon, Juan Li, Jonathan J Finley, Michael Ryan Hansen, Jean-Sébastien Lauret, Elisa Molinari, Xinliang Feng, Johannes V. Barth, Carlos-Andres Palma, Deborah Prezzi, Klaus Müllen, and Akimitsu Narita

J. Am. Chem. Soc., **Just Accepted Manuscript** • DOI: 10.1021/jacs.8b02209 • Publication Date (Web): 19 May 2018

Downloaded from <http://pubs.acs.org> on May 19, 2018

Just Accepted

“Just Accepted” manuscripts have been peer-reviewed and accepted for publication. They are posted online prior to technical editing, formatting for publication and author proofing. The American Chemical Society provides “Just Accepted” as a service to the research community to expedite the dissemination of scientific material as soon as possible after acceptance. “Just Accepted” manuscripts appear in full in PDF format accompanied by an HTML abstract. “Just Accepted” manuscripts have been fully peer reviewed, but should not be considered the official version of record. They are citable by the Digital Object Identifier (DOI®). “Just Accepted” is an optional service offered to authors. Therefore, the “Just Accepted” Web site may not include all articles that will be published in the journal. After a manuscript is technically edited and formatted, it will be removed from the “Just Accepted” Web site and published as an ASAP article. Note that technical editing may introduce minor changes to the manuscript text and/or graphics which could affect content, and all legal disclaimers and ethical guidelines that apply to the journal pertain. ACS cannot be held responsible for errors or consequences arising from the use of information contained in these “Just Accepted” manuscripts.



ACS Publications

is published by the American Chemical Society, 1155 Sixteenth Street N.W., Washington, DC 20036

Published by American Chemical Society. Copyright © American Chemical Society. However, no copyright claim is made to original U.S. Government works, or works produced by employees of any Commonwealth realm Crown government in the course of their duties.

Bandgap Engineering of Graphene Nanoribbons by Control over Structural Distortion

Yunbin Hu^{1,2}, Peng Xie³, Marzio De Corato^{4,5}, Alice Ruini^{4,5}, Shen Zhao⁶, Felix Meggendorfer³, Lasse Arnt Straasø⁷, Loic Rondin⁶, Patrick Simon³, Juan Li^{3,8}, Jonathan J. Finley³, Michael Ryan Hansen⁹, Jean-Sébastien Lauret⁶, Elisa Molinari^{4,5}, Xinliang Feng¹⁰, Johannes V. Barth³, Carlos-Andres Palma³, Deborah Prezzi^{5*}, Klaus Müllen^{1*}, Akimitsu Narita^{1*}

¹Max Planck Institute for Polymer Research, Ackermannweg 10, D-55128 Mainz, Germany.

²Department of Organic and Polymer Chemistry, College of Chemistry and Chemical Engineering, Central South University, Changsha, Hunan 410083, P. R. China.

³Physik-Department, Technische Universität München, James-Frank-Str. 1, D-85748 Garching, Germany.

⁴Dipartimento di Scienze Fisiche, Informatiche e Matematiche, Università di Modena e Reggio Emilia, 41125 Modena, Italy.

⁵Istituto Nanoscienze, CNR, via G. Campi 213/a, 41125, Modena, Italy.

⁶Laboratoire Aimé Cotton, CNRS, Univ. Paris-Sud, ENS Cachan, Université Paris Saclay bat 505 campus d'Orsay, 91405 Orsay cedex, France.

⁷Interdisciplinary Nanoscience Center (iNANO) and Department of Chemistry, Aarhus University, Gustav Wieds Vej 14, DK-8000 Aarhus C, Denmark.

⁸Beijing Institute of Technology, 100081 Beijing, P. R. China.

⁹Institute of Physical Chemistry, Westfälische Wilhelms-Universität Münster, Corrensstr. 28/30, D-48149 Münster, Germany.

¹⁰Center for Advancing Electronics Dresden (cfaed) & Department of Chemistry and Food Chemistry, Technische Universität Dresden, Mommsenstrasse 4, 01062 Dresden, Germany.

ABSTRACT: Amongst organic electronic materials, graphene nanoribbons (GNRs) offer extraordinary versatility as next-generation semiconducting materials for nanoelectronics and optoelectronics due to their tunable properties, including charge-carrier mobility, optical absorption and electronic bandgap, which are uniquely defined by their chemical structures. Although planar GNRs have been predominantly considered until now, non-planarity can be an additional parameter to modulate their property without changing the aromatic core. Herein, we report theoretical and experimental studies on two GNR structures with “cove”-type edges, having an identical aromatic core, but with alkyl side chains at different peripheral positions. The theoretical results indicate that installment of alkyl chains at the innermost positions of the “cove”-type edges can “bend” the peripheral rings of the GNR through steric repulsion between aromatic protons and the introduced alkyl chains. This structural distortion is theoretically predicted to reduce the bandgap by up to 0.27 eV, which is corroborated by experimental comparison of thus synthesized planar and non-planar GNRs through UV-Vis-near infrared absorption and photoluminescence excitation spectroscopy. Our results extend the possibility of engineering GNR properties, adding subtle structural distortion as a distinct and potentially highly versatile parameter.

INTRODUCTION

Strain-induced structural distortions of graphene, the two-dimensional and planar allotrope of carbon, have attracted considerable attention for their significant effect on its electronic structures, electron-phonon coupling and pseudomagnetic field.¹ In particular, the bandgap of graphene can be opened through sufficiently strong

mechanical strain, which is crucial for its application in electronics and optoelectronics.²⁻⁶ Moreover, the segmentation of graphene into quasi-one-dimensional nanostructures, so-called graphene nanoribbons (GNRs), provides a powerful strategy to develop materials with tunable electronic bandgap and paves the way towards GNR-based transistors and other nanoelectronic device elements.⁷⁻¹¹ The effects of non-planarity on the electronic

properties of GNRs have already been addressed in theoretical calculations, which predicted varying bandgap modulation of up to ~ 1 eV, depending on the nature of structural distortion.^{12–16} Experiments in bending GNRs via direct scanning tunneling microscope (STM) manipulation revealed that such structural deformation

indeed affected the electronic band structure.¹⁷ However, such procedures do not allow a control of GNR nonplanarity in a uniform and scalable manner, which is nevertheless essential to establish the new parameter of bandgap engineering for future applications.

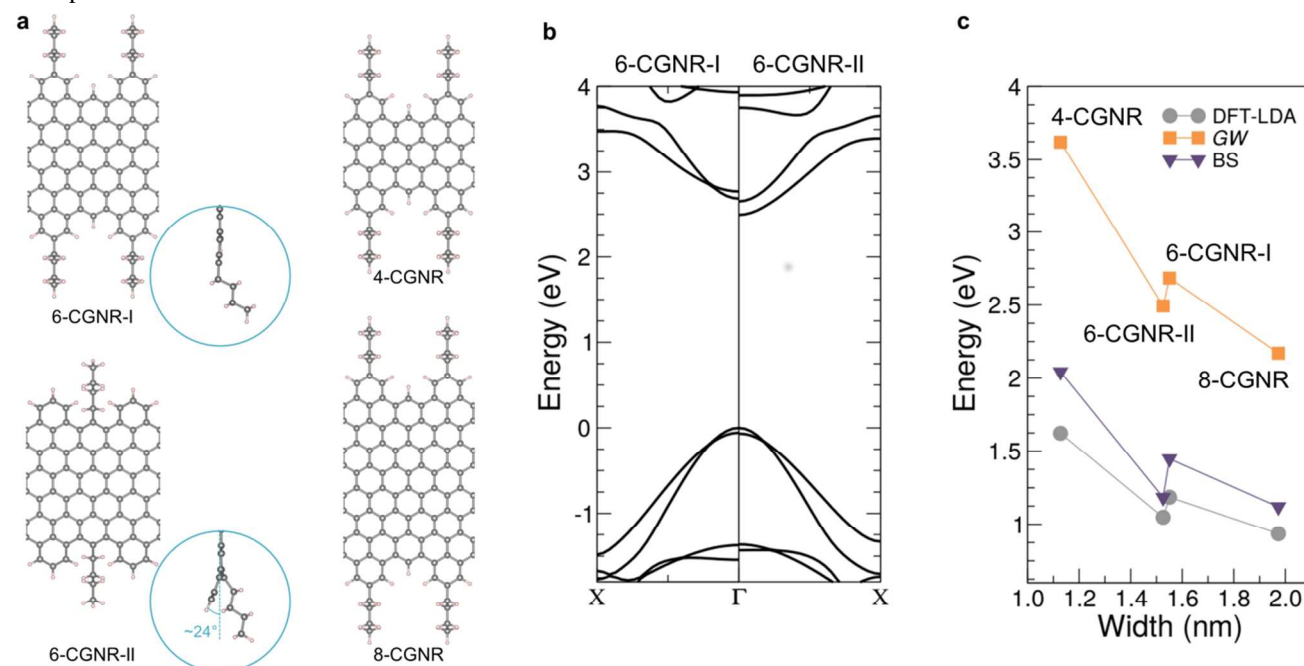


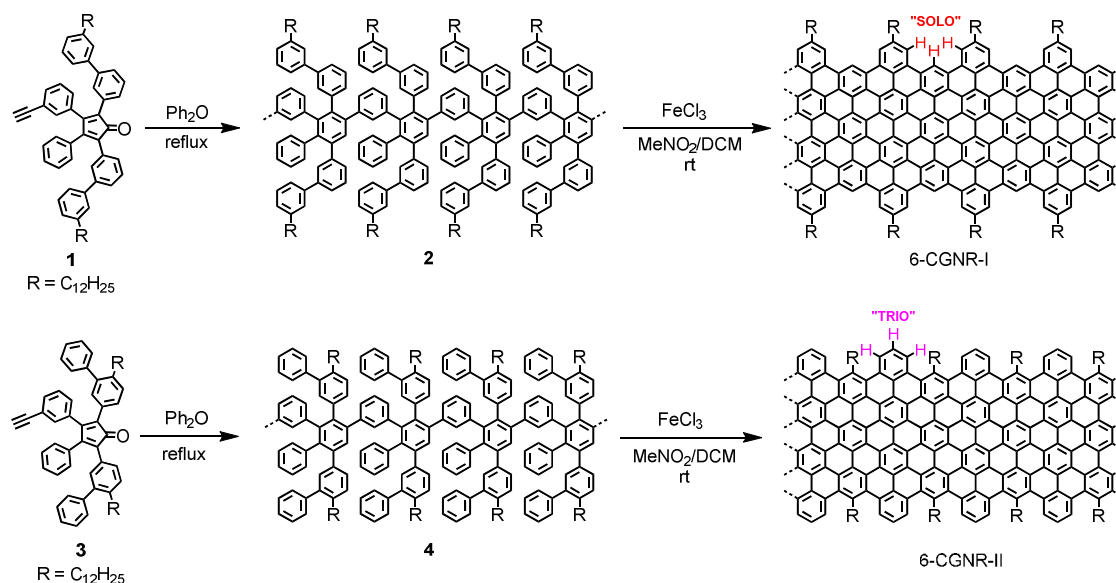
Figure 1. Theoretical models and band structures of the GNRs. (a) Simulated structures of 6-CGNR-I/II, 4-CGNR, and 8-CGNR after the geometrical optimization. The dodecyl chains were replaced with butyl groups for reducing the calculation cost. Insets: Zoom of the side views of 6-CGNR-I/II in the edge region reveal distinct structural distortions. (b) Band structures of 6-CGNR-I/II calculated by the GW method. (c) Fundamental and optical gaps as a function of the width for GNRs that are narrower (4-CGNR) and wider (8-CGNR) than 6-CGNR-I (2.68 eV) and 6-CGNR-II (2.49 eV). The gaps are calculated at different level of theory, i.e. DFT, GW and BS (see Methods Section).

In nanographene chemistry, nanographene molecules, that is large polycyclic aromatic hydrocarbons (PAHs), with non-planar π -surfaces have aroused increasing interest due to their inherent molecular strain, increased solubility, and versatile intermolecular contacts in the bulk phase compared to the planar counterparts.^{18–21} Generally, the non-planarity of nanographene molecules is induced by the presence of nonhexagonal rings and/or sterically crowding edge structures. For example, a grossly warped nanographene with embedded pentagons and heptagons was synthesized by Scott and Itami *et al.*, showing a unique double-concave structure with good solubility.²² Nuckolls *et al.* developed a series of contorted nanographene species with sterically congested cove-shaped peripheries, which revealed fascinating self-assembling and/or charge-transporting properties.¹⁸ Moreover, significant modulation of the electronic structures has also been experimentally demonstrated upon the structural distortion of nanographene molecules in comparison to more planar derivatives with the same aromatic frameworks.^{23, 24} Whereas there is an increasing number of reports on non-planar nanographene molecules, GNRs with well-defined and distorted

structures have remained rare.²⁵ In particular, clear relationships between optical and electronic properties of GNRs induced by deviation from planarity need to be identified toward establishing a rationale in this emerging area.

Herein we have uniformly introduced a strain at the peripheral position of structurally well-defined GNRs with “cove”-type edges (CGNRs) by installing alkyl chains at the innermost positions (6-CGNR-II with the width of 6 carbon atoms at the narrowest), which distort the planarity of the benzo-rings due to steric repulsion against the aromatic protons. From theoretical considerations we infer a significant effect of such structural distortion on the band structure and the optical properties of the GNRs, lowering both optical and electronic bandgaps by 0.2–0.3 eV, compared to the planar 6-CGNR-I substituted at the outermost positions. UV-Vis-near infrared (NIR) absorption and photoluminescence excitation (PLE) spectroscopy analyses of both planar 6-CGNR-I and non-planar 6-CGNR-II have experimentally corroborated the theoretical prediction, revealing a decrease of the optical bandgap by up to 0.27 eV.

Scheme 1. Synthesis of 6-CGNR-I/II through the AB-type Diels–Alder polymerization of tetraphenylcyclopentadienone-based monomers **1 and **3**, respectively, followed by the oxidative cyclodehydrogenation.**



RESULTS AND DISCUSSION

Theoretical study of geometrical and electronic properties of the GNRs. The geometrical optimization of 6-CGNR-I/II by density functional theory (DFT) calculations reveals that the peripheral benzo-rings of 6-CGNR-II are distorted by approximately 24° from planarity, while 6-CGNR-I is completely flat (Figure 1a). Interestingly, the corresponding electronic band structure (Figure 1b), calculated using the *ab initio* GW method, shows a clear band inversion for the lowest two conduction bands, i.e., the second conduction band (v_2) of 6-CGNR-I becomes the lowest conduction band (v_1) of 6-CGNR-II, being lowered by 0.27 eV; the highest valence bands (c_1 and c_2) are instead not significantly modified, resulting in a net decrease of the bandgap of 0.19 eV. Calculations performed both with and without alkyl chains indicate that purely geometrical effects account almost completely for these bandgap differences (see the Supporting Information for details), which result in the different optical spectra shown in Figure 2b (bottom): The lowest energy peak of 6-CGNR-I (1.45 eV), arising from the linear combination of transitions $v_1 \rightarrow c_2$ and $v_2 \rightarrow c_1$, is split for 6-CGNR-II into two peaks (1.18 eV, derived from $v_1 \rightarrow c_1$; 1.39 eV, $v_2 \rightarrow c_2$) as a consequence of the band inversion of conduction bands.

Finally, Figure 1c shows the fundamental and optical gap in vacuum of 6-CGNR-I/II in comparison to 4- and 8-CGNRs^{26, 27} with different widths. The fundamental gap of 6-CGNR-II (2.49 eV) lies in between the gap of 6-CGNR-I (2.68 eV) and that of the wider 8-CGNR (2.17 eV), while the narrowest 4-CGNR shows the largest

fundamental gap (3.62 eV). When the optical properties are compared using the Bethe-Salpeter (BS) approach²⁸ in order to include excitonic effects into the calculations, the effect of the structural distortion is even more pronounced: 6-CGNR-II and 8-CGNR are predicted to have almost the same optical gap (1.18 and 1.12 eV, respectively) whereas 6-CGNR-I shows a gap of 1.45 eV, i.e. 0.27 eV larger than that of 6-CGNR-II. This comparison strongly suggests that the backbone distortion could be used as a design principle to tune the bandgap in addition to the modification of the width.

Bottom-up synthesis of the GNRs. Encouraged by these theoretical results, we have synthesized 6-CGNR-I/II based on the AB-type Diels–Alder polymerization of tetraphenylcyclopentadienone-based monomers **1** and **3**,^{26, 27} followed by oxidative cyclodehydrogenation with iron (III) chloride (Scheme 1; See the Supporting Information for details). Precursors **2** and **4** were prepared with weight-average molecular weights (M_w) of 64–125 and 61–121 kg/mol and polydispersity index (PDI) of 1.4–1.5 and 1.6–1.8, respectively, based on size-exclusion chromatography (SEC) analyses against poly(*p*-phenylene) (PPP) and polystyrene (PS) standards, which were previously shown to be appropriate for the analysis of such precursors.²⁶ The relatively small M_w values, compared with the highest values reported for previous systems,^{26, 27} were selected to obtain 6-CGNR-I/II with higher processability, while having estimated lengths of approximately 100 nm, after the oxidative cyclodehydrogenation.

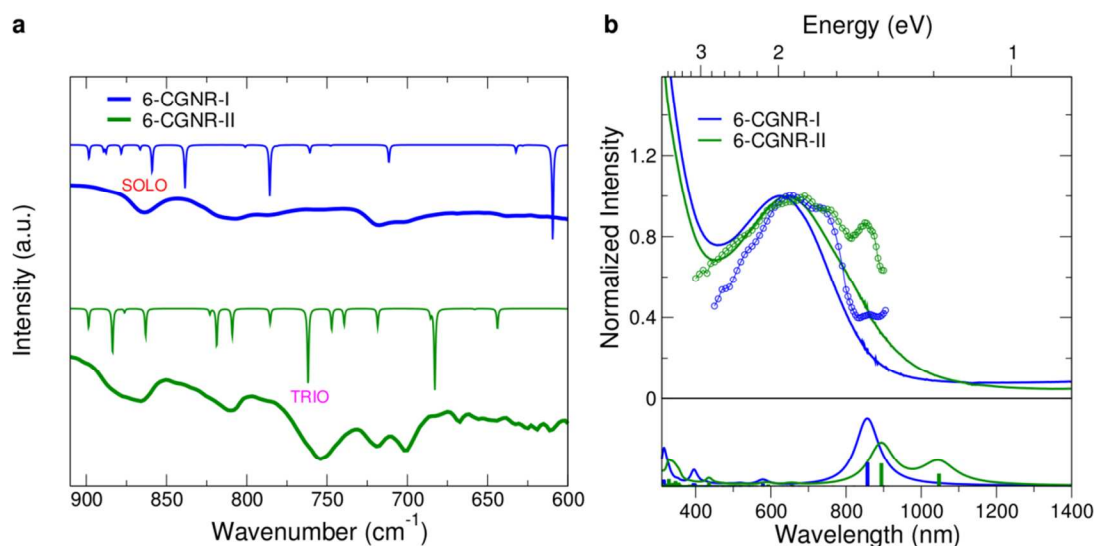


Figure 2. Spectroscopic characterization of GNRs. (a) FTIR spectra of 6-CGNR-I/II (plain line: simulation; bold line: measured on powder samples). (b) Experimental (top) UV-vis-NIR absorption (solid lines) and photoluminescence excitation (solid lines with hollow circles) spectra of 6-CGNR-I/II, recorded with dispersions in 1,2,4-trichlorobenzene (TCB). DFT GW-BS simulated (bottom) UV-vis-NIR absorption of the isolated ideal 6-CGNR-I/II in vacuum.

Bulk spectroscopic characterizations of the GNRs.

6-CGNR-I/II were initially characterized by Fourier transform infrared (FTIR), Raman, solid-state NMR, and UV-vis-NIR absorption spectroscopies (Figures 2 and S6-S12). The FTIR spectra of 6-CGNR-I/II are significantly different despite having the same aromatic core structure, indicating considerable effects of the peripheral substitutions on the vibrational properties of the GNRs (Figure 2a). IR spectra simulated by means of the density-functional perturbation theory (DFPT) method indeed elucidated distinct modes arising from the structures of 6-CGNR-I/II in view of their different edge morphology. 6-CGNR-I is characterized by the SOLO modes (839 and 859 cm^{-1} , wagging of single CH groups, Figure 2a),²⁸ which are supposed to be absent in 6-CGNR-II. However, we find a peak at about the same frequency (863 cm^{-1}) in the spectrum of 6-CGNR-II, which is not edge-specific but involves the carbon backbone according to our calculations and the analysis of the displacements. Despite the different origin, which is fully understood within our theoretical analysis (see Supporting Information for further details), this mode would not allow to distinguish the two structures. The most relevant mode to fingerprint the two structures is the so-called TRIO mode (762 cm^{-1} , wagging of triply-adjacent CH groups, Figure 2),²⁹ which dominates the spectrum of 6-CGNR-II, while it is absent in the spectrum of 6-CGNR-I. The experimental spectra are evidently different for 6-CGNR-I and 6-CGNR-II, and overall in good agreement with the theoretical results, supporting the successful synthesis and the structural variation. The Raman spectra of 6-CGNR-I/II are

consistent with those of previously reported bottom-up synthesized GNRs, which showed intense first-order D and G peaks as well as second-order peaks (Figure S9).^{26, 27, 30} 2D solid-state ^1H - ^1H double-quantum-single-quantum (DQ-SQ) magic-angle-spinning (MAS) NMR correlation and 1D $^{13}\text{C}\{^1\text{H}\}$ recoupled polarization heteronuclear single quantum correlation (REPT-HSQC) MAS NMR spectra of 6-CGNR-I/II were comparable to those of previously reported GNRs, providing further evidences for the formation of GNRs (see the Supporting Information for details).^{26, 27}

With the long alkyl chains densely installed at the peripheral positions, both 6-CGNR-I/II can be dispersed in organic solvents such as tetrahydrofuran, chlorobenzene and 1,2,4-trichlorobenzene (TCB). UV-vis-NIR absorption and photoluminescence excitation spectra of 6-CGNR-I/II are thus recorded using dispersions in TCB (Figure 2b). 6-CGNR-I showed a broad absorption band with a maximum at 624 nm and onset at $867\pm 10\text{ nm}$, corresponding to an optical gap of $1.43\pm 0.02\text{ eV}$. In comparison, 6-CGNR-II exhibited a red-shifted and broader absorption pattern with a long-wavelength absorption maximum at 649 nm and absorption onset at $990\pm 10\text{ nm}$, which corresponds to an optical gap of $1.25\pm 0.02\text{ eV}$. This optical gap value of 6-CGNR-II is around 0.18 eV smaller than that of 6-CGNR-I and even closer to the value previously reported for 8-CGNR, namely $1.24\pm 0.03\text{ eV}$.²⁷ This trend follows the simulated gas-phase optical gap discussed above (Figure 1c).

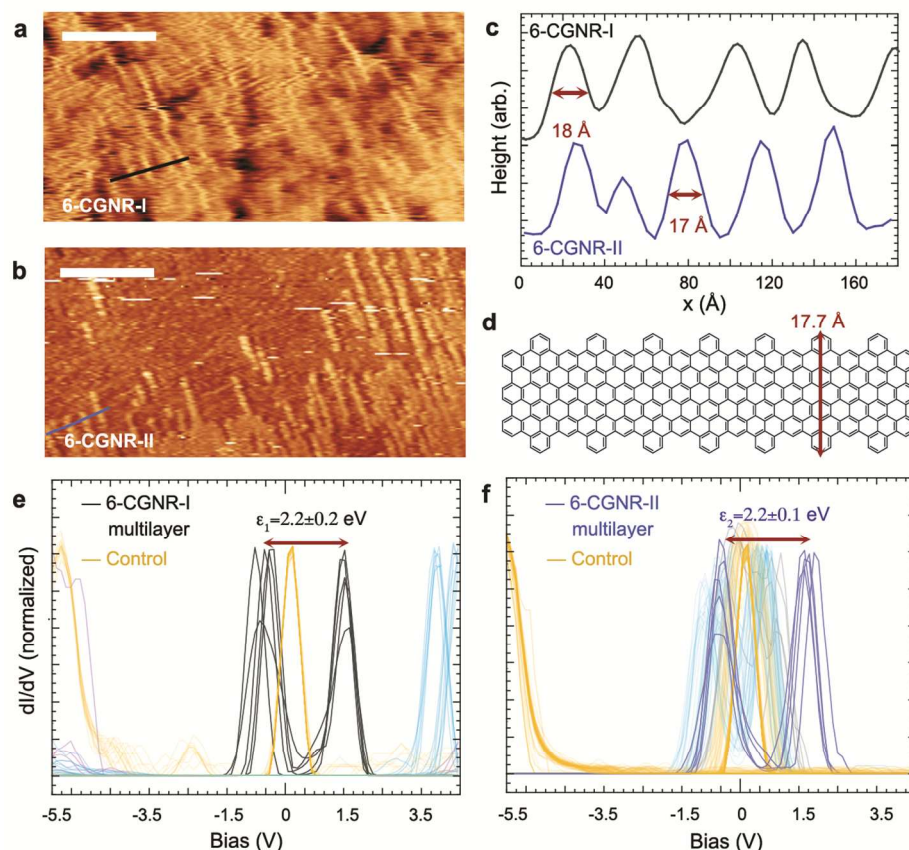


Figure 3. Surface optical and electronic gap of GNRs on diamond. (a,b) STM data of deposited samples of 6-CGNR-I ($V_s = -100$ mV, $I_t = 10$ pA) and 6-CGNR-II ($V_s = 300$ mV, $I_t = 30$ pA) on H-C(100), respectively. (c) Profiles for 6-CGNR-I (blue line) and 6-CGNR-II (black line) show selected FWHMs of ~ 17 Å and ~ 18 Å, respectively, in agreement with (d) the width of the conjugated aromatic core (17.7 Å). The inter-GNR distance varies presumably due to different absorption geometries of the alkyl chains. (e,f) Histogram-filtered (see text) STS on the ultrathin films of 6-CGNR-I/II on O-C(100) by employing a sharp STM tip close to gold top-electrodes (see Figures S16-S17). Scale bars (a,b) 20 nm.

The PL excitation spectra of both 6-CGNR-I and -II roughly agree with the UV-vis-NIR spectra around the absorption maxima while showing a shoulder at ~ 750 nm (~ 1.65 eV). On the other hand, 6-CGNR-II exhibits an extra peak at 853 nm (1.45 eV), where the excitation spectrum of 6-CGNR-I is featureless. The absorption spectra seem to be consistent with this observation, with 6-CGNR-II having a shoulder peak at approximately 850 nm, which contributes to the broadening of the spectrum and lowering of the optical gap (Figure 3a, top). The lowest energy peak in the 6-CGNR-I (-II) PL excitation spectrum of the dispersions in TCB appears blue-shifted by ~ 0.20 eV (~ 0.27 eV) with respect to the GW-BS calculated optical spectra of the isolated ideal GNRs (Figure 3b, bottom), as previously reported for other GNRs.^{31,32} Such a rigid shift on the lowest energy excitations can be partly traced back to the 0.1-0.2 accuracy of our method.²⁸ Higher-energy peaks are instead well-known to be less reproducible, being more sensitive to environmental effects. Indeed, effects, such as aggregation,^{33,34} conformational disorder,³⁵ interaction with long side chains³⁶ and with solvent molecules,³⁷ may partly contribute to deviations from ideally calculated optical spectra. Importantly, the calculated optical spectra

elucidate two separate optical transitions for 6-CGNR-II and only one for 6-CGNR-I, in clear agreement with the experimental observations (Figure 3b). These results further highlight the striking differences in the excitonic gaps of 6-CGNR-I/II, consequence of minimal structural engineering, and the suitability of this strategy to tailor GNR optical and electronic properties for technological applications.

Characterizations of the GNRs on diamond surfaces. Diamond substrates with atomically flat surfaces grant access to simultaneous measurement of optical, electronic and morphological properties by means of UV-vis-NIR absorption, scanning tunneling spectroscopy (STS) and STM, respectively. To this end, we deposited 6-CGNR-I/II from dispersions in TCB on hydrogen and oxygen terminated diamond surfaces (O-C(100) and H-C(100), respectively). The substrates were then dried and ultrasonicated in isopropanol until the corresponding absorption of 6-CGNR-I/II was only $0.010 \pm 0.004\%$ (see Methods and Figure S13). STM measurements of 6-CGNR-I films cast on H-C(100) show rather disordered multilayers of ribbon-shaped objects (Figure 3a). In contrast, monolayers and bilayers of 6-CGNR-II could be recorded with relative ease (Figure

3b), extending over micrometer sized areas (Figure S14). The higher processability of 6-CGNN-II is presumably due to less efficient interaction of non-planar 6-CGNN-II, compared to the planar 6-CGNN-I. The average full width at half maximum (FWHM) of the observed features amounts to 18 ± 2 Å for both GNNs (Figure 3c), in agreement with the molecular modeling of the aromatic core (H to H distance of 17.7 Å, Figure 3d). The average length of observed ribbons is close to 20 nm, which is shorter than the estimated ~100 nm, but typical of broader GNNs deposited from dispersions, most probably because longer ribbons with lower dispersibility cannot be dispersed into the solvent.²⁷

UV-Vis-NIR spectroscopy of the ultrathin films of 6-CGNN-I/II on the O-C(100) surface reveals comparable absorption profiles to those in dispersions with absorption maxima of 580 ± 5 and 640 ± 5 nm, respectively (Figure S15e). These values are slightly blue-shifted compared with their absorption maxima in dispersions (624 nm for 6-CGNN-I and 649 nm for 6-CGNN-II), which can be explained by red-shift of the absorption spectra in dispersions due to the interaction of the GNNs with the solvent TCB molecules.³⁸ Bulk films also showed the absorption maxima at comparable wavelengths (6-CGNN-I: 610 nm; 6-CGNN-II: 650 nm; solid lines in Figure S15e). These results, reveal that the key properties persist in interfacial and thin film environments and further validate that the experimentally observed modulation of the optical properties are intrinsic effects of structural distortion as predicted by the theory.

STS analysis of the electronic bandgap of 6-CGNN-I/II was challenging, because the STS-measured resonance onset of H-C(100) is close to 1.0 V,³⁹ which obscured molecular resonant signals at this energy. Nevertheless, benefiting instead from the oxygen terminated diamond O-C(100) having an STS-measured conduction band onset >4 V sample bias,⁴⁰ we could record tunneling spectra at the diamond-GNN film interface (Figure S16-17), although only multilayers of GNNs could be obtained on this surface (see Methods and Supporting Information for the experimental details). Figures 3e and 3f show the normalized dI/dV of histogram-filtered data (see also Figure S18) including >1000 STS curves collected from several STS junctions near the gold electrodes. The coloring of the curves is automatically performed by a histogram script. The yellow curve color is related to STS data common to control samples without GNNs: signals close to -4 V are assigned to diamond while signals close to zero bias are due to Pt-Ir tip-gold short-circuits, encountered when the junctions are formed close to the gold electrodes (see Figures S16-S17). The histogram-filter further extracts several signals, which we assign to the valence and conduction band of 6-CGNN-I (Figure 3e, black) and 6-CGNN-II (Figure 3f, blue). Some additional signals are also extracted by the histogram filter (Figure 3e and 3f, in cyan), which might be related to supramolecular stacking effects of the GNNs in multilayers. The multilayer character of the samples, also increasing the dielectric screening on substrate, did not

allow the precise determination of the ~0.2 eV gap difference between 6-CGNN-I and 6-CGNN-II by the current STS method. Nevertheless, the electronic gap of ~2.2 eV could be measured for both 6-CGNN-I and 6-CGNN-II. Considering dielectric screening by the substrate which lowers the electronic bandgap, these results are consistent with the calculated gaps of 2.5–2.7 eV in gas-phase. Further experiments to achieve atomic structural characterization by STM, employing electrospray ionization deposition under ultrahigh vacuum conditions, are ongoing in our laboratories.

CONCLUSION

In summary, we have achieved the bottom-up synthesis of planar 6-CGNN-I and non-planar 6-CGNN-II with the same aromatic core structure, which were validated by a combination of IR, Raman, solid-state NMR, STM and STS analysis. Theoretical studies employing the GW-BS approach and UV-vis-NIR absorption and photoluminescence excitation spectra identify a bandgap compression of 6-CGNN-II relative to 6-CGNN-I by ~0.2 eV, which is associated with a lowering of the conduction band through structural distortions. These results indicate that the electronic and optical properties of GNNs can be generally modulated not only by changing the aromatic backbone structure, doping with heteroatoms, and/or by installing functional groups at the edges, but also by introducing systematic and uniform deviations from planarity. Thus the bandgap can be lowered simply by making the GNNs non-planar, in contrast to our previous approach to laterally extend the GNNs, namely to 8-CGNN (see Figure 1), which significantly decreases the processability. Our results also suggest that the non-planarity enhances the processability of 6-CGNN-II in comparison to the planar 6-CGNN-I, most probably because the interaction between the GNNs can be hindered by the non-planar peripheries.⁴¹ Moreover, the further development of our strategy will also allow for tailoring the degree of structural distortion by attaching substitutions with different bulkiness, which is expected to enable the fine-tuning of the bandgaps and other parameters. Considering the fact that there are thus far only a few examples of GNNs that could be made longer than 100 nm with high yield, mainly relying on the AB-type Diels-Alder polymerization in solution, this new tool for engineering the GNN properties is suggested to be highly valuable for the future development of GNN-based nanoelectronics and optoelectronics.

METHODS SECTION

Sample preparation. Full details regarding the synthesis and standard characterization of all the materials are given in the Supporting Information.

Theoretical calculations. Simulations of the ground-state structural and vibrational properties were performed using a first-principle supercell implementation of Density-Functional Theory (DFT) and Density-Functional Perturbation Theory (DFPT)⁴² based

on plane waves and pseudopotentials, together with the choice of the LDA exchange-correlation functional, as available in the Quantum ESPRESSO package.⁴³ The DFT-LDA band structures and optical spectra were improved by introducing many-body corrections (i.e. electron-electron and electron-hole interactions) within the GW-BS framework.²⁸ Calculations were performed by using the YAMBO code.⁴⁴ Both vibrational and optical properties were simulated for gas-phase GNRs functionalized with shorter alkyl chains, i.e. ethyl or butyl groups instead of dodecyl groups, in order to make them more computationally affordable. We have checked that this approximation does not affect the characterization of the properties of interest, as detailed in the Supporting Information.

Excitation spectra. The excitation spectra of both GNR 1 and GNR 2 have been recorded in solution using a supercontinuum laser (Fianium) filtered either by a monochromator or an AOTF filter. The luminescence is detected on the low energy tail of the spectrum.

STM and STS measurements. Scanning tunneling microscopy (STM, Agilent Technologies 5100) was employed to probe the C(100) interface either in constant current imaging mode or in spectroscopy mode (STS) (STS, see below) with a current compliance of 10 nA. Prior to STS measurements employing a specialized setup (see below and Figure S16-S17), a suitable tunneling regime was identified by recording STM data of the 6-CGNRs ($V_s \sim 500$ mV, $I_t \sim 20$ pA) or measuring the diamond O-C(100) band onset ($V_s \sim 5.5$ V, $I_t \sim 20$ pA) in control samples. Details regarding sample preparation are provided in the Supporting Information.

ASSOCIATED CONTENT

Supporting Information. Experimental and theoretical details, characterization of polyphenylene precursors, Raman and solid-state NMR analysis spectra, additional FTIR and UV-vis-NIR spectra, further details of the STM and STS analysis, and ¹H and ¹³C NMR spectra. This material is available free of charge via the Internet at <http://pubs.acs.org>.

AUTHOR INFORMATION

Corresponding Authors

deborah.prezzi@nano.cnr.it
muellen@mpip-mainz.mpg.de
narita@mpip-mainz.mpg.de

Notes

The authors declare no competing financial interests.
the manuscript.

ACKNOWLEDGMENT

We are grateful to Wei Ran for the microfabrication, and to Jose A. Garrido and Martin Stutzmann for kindly providing the diamond C(100) substrate and infrastructure support at the Walter Schottky Institute. This work was financially supported by the Max Planck Society, ERC grant on NANOGRAPH, DFG Priority Program SPP 1459, the European Commission through the FET-Proactive Project

“MoQuaS” (contract number 610449), the FET-Open Project “2D Ink” (664878) and Graphene Flagship. D.P. acknowledges support from the European Union H2020-EINFRA-2015-1 program (Grant No. 676598, project “MaX - materials at the exascale”). Computational resources were granted by the Center for Functional Nanomaterials at Brookhaven National Laboratory, supported by the U.S. Department of Energy, Office of Basic Energy Sciences, under contract number DE-SC0012704. JS Lauret is partially funded by “Institut Universitaire de France”. M.R.H. acknowledges financial support from the Villum Foundation under the Young Investigator Programme (VKR023122)

REFERENCES

- (1) Si, C.; Sun, Z.; Liu, F. *Nanoscale* **2016**, *8*, 3207-3217.
- (2) Pereira, V. M.; Castro Neto, A. H.; Peres, N. M. R. *Phys. Rev. B* **2009**, *80*, 045401.
- (3) Choi, S.-M.; Jhi, S.-H.; Son, Y.-W. *Phys. Rev. B* **2010**, *81*, 081407(R).
- (4) Farjam, M.; Rafii-Tabar, H. *Phys. Rev. B* **2009**, *80*, 167401.
- (5) Ribeiro, R. M.; Pereira, V. M.; Peres, N. M. R.; Briddon, P. R.; Castro Neto, A. H. *New J. Phys.* **2009**, *11*, 115002.
- (6) Cocco, G.; Cadelano, E.; Colombo, L. *Phys. Rev. B* **2010**, *81*, 241412(R).
- (7) Chen, L.; Hernandez, Y.; Feng, X.; Müllen, K. *Angew. Chem. Int. Ed.* **2012**, *51*, 7640-7654.
- (8) Narita, A.; Feng, X.; Müllen, K. *Chem. Rec.* **2015**, *15*, 295-309.
- (9) Xu, W.; Lee, T.-W. *Mater. Horiz.* **2016**, *3*, 186-207.
- (10) Novoselov, K. S.; Fal'ko, V. I.; Colombo, L.; Gellert, P. R.; Schwab, M. G.; Kim, K. *Nature* **2012**, *490*, 192-200.
- (11) Bennett, P. B.; Pedramrazi, Z.; Madani, A.; Chen, Y.-C.; De Oteyza, D. G.; Chen, C.; Fischer, F. R.; Crommie, M. F.; Bokor, J. *Appl. Phys. Lett.* **2013**, *103*, 253114.
- (12) Koskinen, P. *Phys. Rev. B* **2012**, *85*, 205429.
- (13) Sun, L.; Li, Q.; Ren, H.; Su, H.; Shi, Q. W.; Yang, J. *J. Chem. Phys.* **2008**, *129*, 074704.
- (14) Peng, X.; Velasquez, S. *Appl. Phys. Lett.* **2011**, *98*, 023112.
- (15) Lu, Y.; Guo, J. *Nano Res.* **2010**, *3*, 189-199.
- (16) Cocchi, C.; Prezzi, D.; Ruini, A.; Caldas, M. J.; Molinari, E. *J. Phys. Chem. C* **2012**, *116*, 17328-17335.
- (17) van der Lit, J.; Jacobse, P. H.; Vanmaekelbergh, D.; Swart, I. *New J. Phys.* **2015**, *17*, 053013.
- (18) Ball, M.; Zhong, Y.; Wu, Y.; Schenck, C.; Ng, F.; Steigerwald, M.; Xiao, S.; Nuckolls, C. *Acc. Chem. Res.* **2015**, *48*, 267-276.
- (19) Pascal, R. A. *Chem. Rev.* **2006**, *106*, 4809-4819.
- (20) Wu, Y.-T.; Siegel, J. S. *Chem. Rev.* **2006**, *106*, 4843-4867.
- (21) Narita, A.; Wang, X.-Y.; Feng, X.; Müllen, K. *Chem. Soc. Rev.* **2015**, *44*, 6616-6643.
- (22) Kawasumi, K.; Zhang, Q.; Segawa, Y.; Scott, L. T.; Itami, K. *Nat. Chem.* **2013**, *5*, 739-744.
- (23) Baumgärtner, K.; Meza Chinchá, A. L.; Dreuw, A.; Rominger, F.; Mastalerz, M. *Angew. Chem. Int. Ed.* **2016**, *55*, 15594-15598.
- (24) Wasserfallen, D.; Kastler, M.; Pisula, W.; Hofer, W. A.; Fogel, Y.; Wang, Z.; Müllen, K. *J. Am. Chem. Soc.* **2006**, *128*, 1334-1339.
- (25) Liu, J.; Li, B.-W.; Tan, Y.-Z.; Giannakopoulos, A.; Sanchez-Sanchez, C.; Beljonne, D.; Ruffieux, P.; Fasel, R.; Feng, X.; Müllen, K. *J. Am. Chem. Soc.* **2015**, *137*, 6097-6103.
- (26) Narita, A.; Feng, X.; Hernandez, Y.; Jensen, S. A.; Bonn, M.; Yang, H.; Verzhbitskiy, I. A.; Casiraghi, C.; Hansen, M. R.; Koch, A. H.; Fytas, G.; Ivasenko, O.; Li, B.; Mali, K. S.

Balandina, T.; Mahesh, S.; De Feyter, S.; Müllen, K. *Nat. Chem.* **2014**, *6*, 126-132.

(27) Narita, A.; Verzhbitskiy, I. A.; Frederickx, W.; Mali, K. S.; Jensen, S. A.; Hansen, M. R.; Bonn, M.; De Feyter, S.; Casiraghi, C.; Feng, X.; Müllen, K. *ACS Nano* **2014**, *8*, 11622-11630.

(28) Onida, G.; Reining, L.; Rubio, A. *Rev. Mod. Phys.* **2002**, *74*, 601-659.

(29) Centrone, A.; Brambilla, L.; Renouard, T.; Gherghel, L.; Mathis, C.; Müllen, K.; Zerbi, G. *Carbon* **2005**, *43*, 1593-1609.

(30) Verzhbitskiy, I. A.; De Corato, M.; Ruini, A.; Molinari, E.; Narita, A.; Hu, Y.; Schwab, M. G.; Bruna, M.; Yoon, D.; Milana, S.; Feng, X.; Müllen, K.; Ferrari, A. C.; Casiraghi, C.; Prezzi, D. *Nano Lett.* **2016**, *16*, 3442-3447.

(30) Abbas, A. N.; Liu, G.; Narita, A.; Orosco, M.; Feng, X.; Müllen, K.; Zhou, C. *J. Am. Chem. Soc.* **2014**, *136*, 7555-7558.

(31) Denk, R.; Hohage, M.; Zeppenfeld, P.; Cai, J.; Pignedoli, C. A.; Söde, H.; Fasel, R.; Feng, X.; Müllen, K.; Wang, S.; Prezzi, D.; Ferretti, A.; Ruini, A.; Molinari, E.; Ruffieux, P. *Nat. Commun.* **2014**, *5*, 4253.

(32) Denk, R.; Lodi-Rizzini, A.; Wang, S.; Hohage, M.; Zeppenfeld, P.; Cai, J.; Fasel, R.; Ruffieux, P.; Berger, R. F. J.; Chen, Z.; Narita, A.; Feng, X.; Müllen, K.; Biagi, R.; De Renzi, V.; Prezzi, D.; Ruini, A.; Ferretti, A. *Nanoscale* **2017**, *9*, 18326-18333.

(33) Samanta, S.; Chaudhuri, D. *J. Phys. Chem. Lett.* **2017**, *8*, 3427-3432.

(34) Li, Y.; Jia, Z.; Xiao, S.; Liu, H.; Li, Y. *Nat. Commun.* **2016**, *7*, 11637.

(35) Chamberlain, T. W.; Biskupek, J.; Rance, G. A.; Chuvilin, A.; Alexander, T. J.; Bichoutskaia, E.; Kaiser, U.; Khlobystov, A. N. *ACS Nano*, **2012**, *6*, 3943-3953.

(36) Saathoff, J. D.; Clancy, P. J. *Phys. Chem. B* **2015**, *119*, 4766-4776.

(37) Ohno, Y.; Iwasaki, S.; Murakami, Y.; Kishimoto, S.; Maruyama, S. *Phys. Status Solidi B Basic Solid State Phys.* **2007**, *244*, 4002-4005.

(38) Abbas, A. N.; Liu, G.; Narita, A.; Orosco, M.; Feng, X.; Müllen, K.; Zhou, C. *J. Am. Chem. Soc.* **2014**, *136*, 7555-7558.

(39) Li, J.; Wieghold, S.; Öner, M. A.; Simon, P.; Hauf, M. V.; Margapoti, E.; Garrido, J. A.; Esch, F.; Palma, C.-A.; Barth, J. V. *Nano Lett.* **2014**, *14*, 4486-4492.

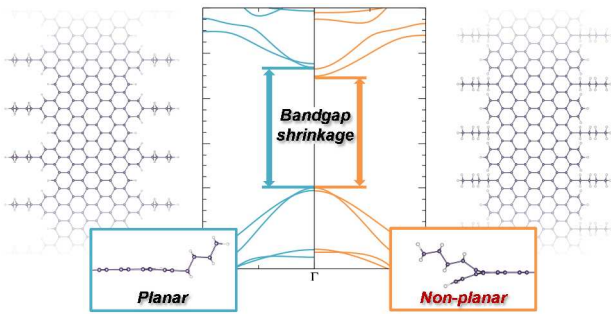
(40) Bobrov, K.; Mayne, A. J.; Dujardin, G. *Nature* **2001**, *413*, 616-619.

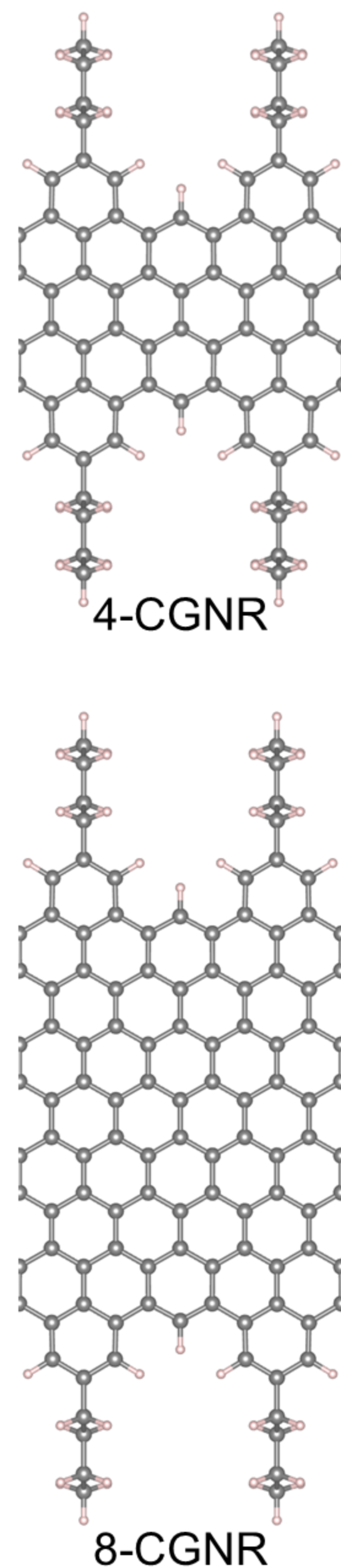
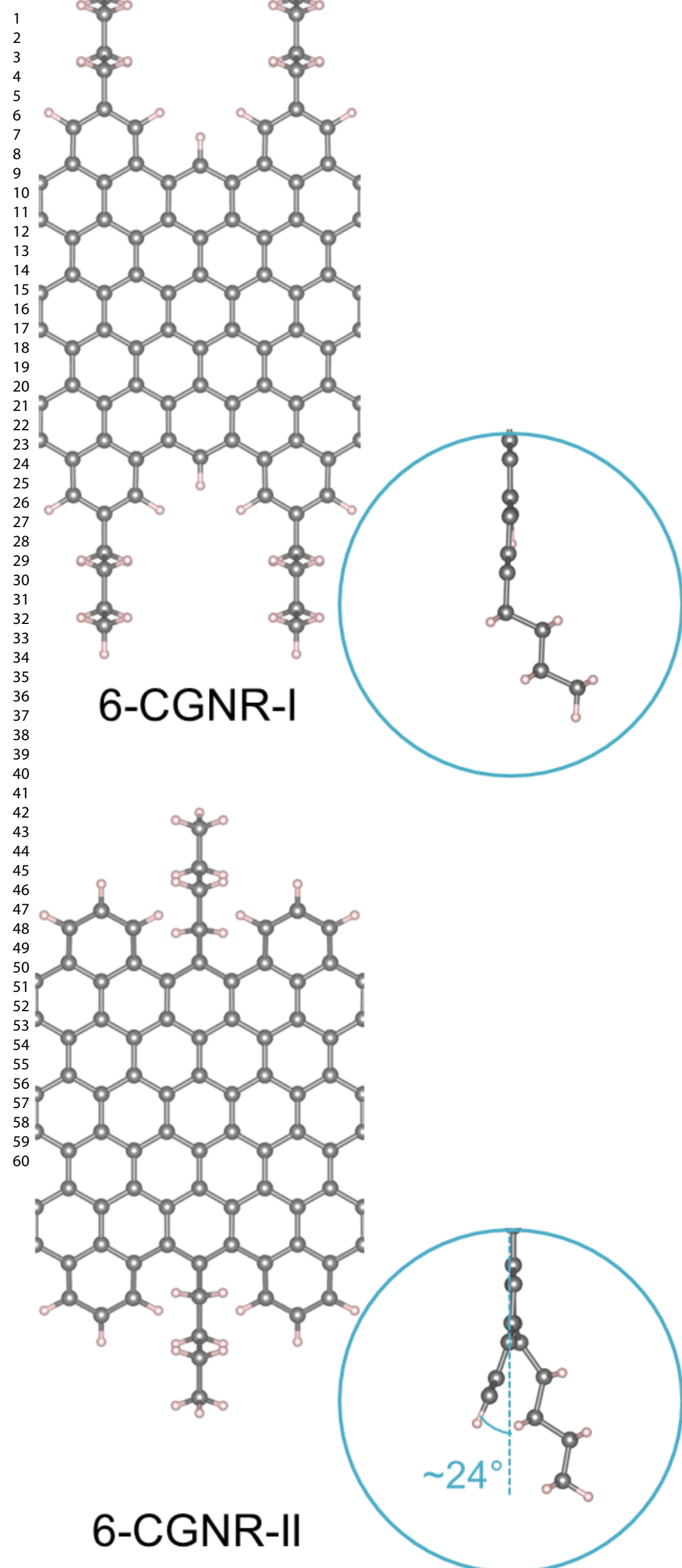
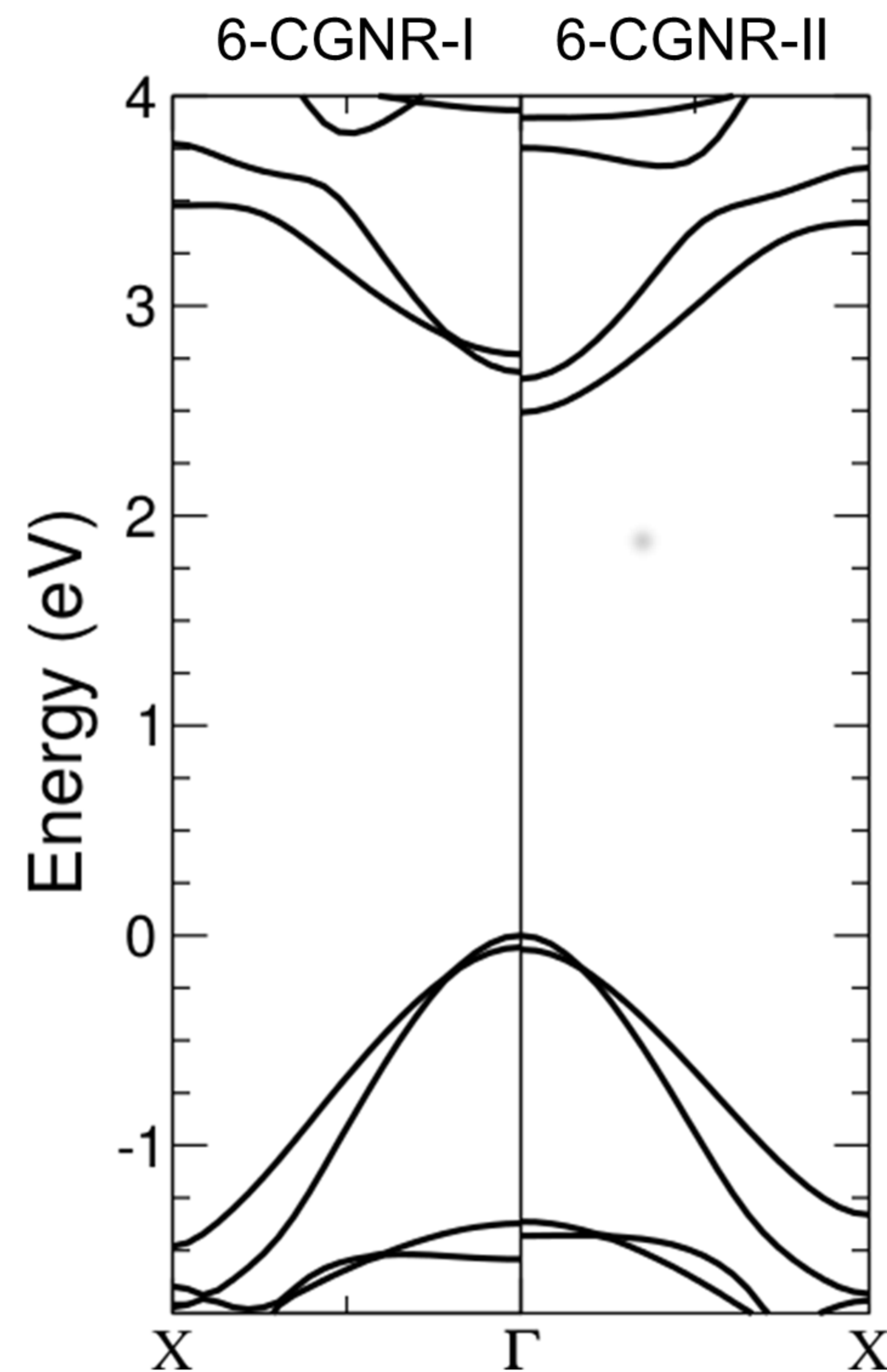
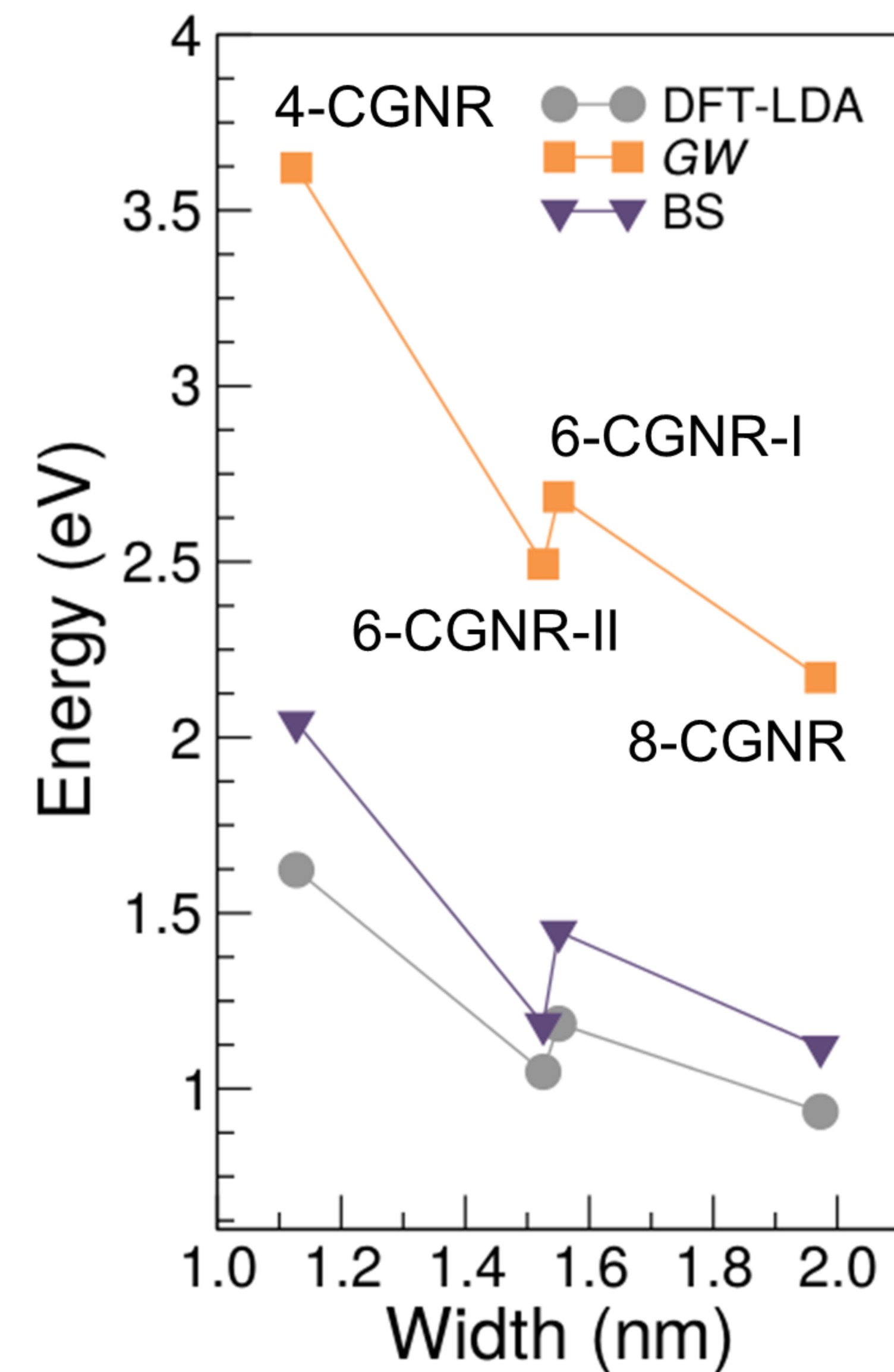
(41) Tan, Y.-Z.; Yang, B.; Parvez, K.; Narita, A.; Osella, S.; Beljonne, D.; Feng, X.; Müllen, K. *Nat. Commun.* **2013**, *4*, 2646.

(42) Baroni, S.; De Gironcoli, S.; Dal Corso, A.; Giannozzi, P. *Rev. Mod. Phys.* **2001**, *73*, 515-562.

(43) Giannozzi, P.; Baroni, S.; Bonini, N.; Calandra, M.; Car, R.; Cavazzoni, C.; Ceresoli, D.; Chiarotti, G. L.; Cococcioni, M.; Dabo, I.; Dal Corso, A.; De Gironcoli, S.; Fabris, S.; Fratesi, G.; Gebauer, R.; Gerstmann, U.; Gougoussis, C.; Kokalj, A.; Lazzeri, M.; Martin-Samos, L.; Marzari, N.; Mauri, F.; Mazzeo, R.; Paolini, S.; Pasquarello, A.; Paulatto, L.; Sbraccia, C.; Scandolo, S.; Sclauzero, G.; Seitsonen, A. P.; Smogunov, A.; Umari, P.; Wentzcovitch, R. M. *J. Phys. Condens. Mater* **2009**, *21*, 395502.

(44) Marini, A.; Hogan, C.; Grüning, M.; Varsano, D. *Comput. Phys. Commun.* **2009**, *180*, 1392-1403.



a**b****c**

1
2
3
4
5
6
7
8
9
10
11
12
13
14
15
16
17
18
19
20
21
22
23
24
25
26
27
28
29
30
31
32
33
34
35
36
37
38
39
40
41
42
43

